Title

Magnetization reversal of Co/Pt multilayers: Microscopic origin of high-field magnetic irreversibility

Journal

Physical Review B, 70(22)

ISSN

1098-0121

Authors

Davies, J E
Hellwig, O
Fullerton, E E
et al.

Publication Date

2004-12-01

Peer reviewed

Magnetization Reversal of Co/Pt Multilayers: Microscopic Origin of High Field Magnetic Irreversibility

Joseph E. Davies[1], Olav Hellwig[2,3], Eric E. Fullerton[3], Greg Denbeaux[4,5], J. B. Kortright[4] and Kai Liu[1,*]

[1]Physics Department, University of California, Davis, CA 95616, USA

[2]BESSY GmbH, 12489 Berlin, Germany

[3]San Jose Research Center, Hitachi Global Storage Technologies, San Jose, CA 95120, USA

[4]Materials Science Division, Lawrence Berkeley National Laboratory, Berkeley, CA 94720, USA

[5]College of Nanoscale Science and Engineering, University at Albany, Albany, NY 12203, USA

We investigate the magnetization reversal in $[Co(4Å)/Pt(7Å)]_{50}$ multilayers with perpendicular magnetic anisotropy both macroscopically by First Order Reversal Curve (FORC) technique and microscopically by Transmission X-Ray Microscopy (TXRM) and resonant x-ray Small Angle Scattering (SAS). In particular, we focus on the nucleation and saturation processes. The onset of magnetization reversal is dominated by irreversible processes corresponding to the avalanche-like propagation of 1-dimensional stripe domains that originate from earlier nucleated 0-dimensional bubble domains. In a second stage we observe mainly reversible behavior where the overall domain topology is preserved. Finally another irreversible process brings the sample to negative saturation, corresponding to the contraction and annihilation of domains. Interestingly, even well beyond the apparent major-loop saturation field, the FORC diagram exhibits pronounced irreversible switching and thus provides a direct measure of the true (and significantly higher) saturation field. TXRM and SAS measurements reveal on a microscopic level that some residual bubble domains with negligible moments still persist for fields well above the apparent saturation field. These residual domains, if un-annihilated, significantly alter the subsequent magnetization reversal.

PACS: 75.60.-d, 75.70.Kw, 75.70.Cn, 68.37.Yz

I. Introduction

In recent years there has been tremendous interest in magnetic nanostructures, largely due to advances in the fields of magneto-electronics and magnetic recording [1]. Central to the investigation of magnetic nanostructures are hysteresis and magnetization reversal processes. Fundamentally, the reversible vs. irreversible magnetization switching often are manifestations of the microscopic magnetic interactions. For example, the reversible switching in spring magnets is a result of low crystalline anisotropy and interlayer coupling [2]; the irreversible switching in exchange biased systems could be due to interfacial pinning by antiferromagnetic domains [3,4]. Technologically, the reversal characteristics, such as onset and endpoint of switching, and the distribution of switching fields, are critical to devices that consist of large arrays of magnetic entities, such as magnetic random access memory [5] and patterned magnetic recording media [6].

In this work, we employ a First Order Reversal Curve (FORC) technique [7-10] to examine the macroscopic magnetization reversal processes in Co/Pt multilayers, in particular the degree of reversible vs. irreversible switching. To probe the microscopic origin of this behavior we exploit Transmission X-Ray Microscopy (TXRM) and resonant magnetic x-ray Small Angle Scattering (SAS). The Co/Pt multilayers chosen are an important material system due to their perpendicular magnetic anisotropy and potential applications as future high-density magnetic recording media [11-14]. We distinguish three distinct stages during a complete reversal from positive to negative saturation: an initial irreversible process due to domain nucleation and primarily domain propagation, then an extended reversible stage as the domains expand/contract in width without changing their topography, and finally another irreversible process corresponding to the annihilation of domains. Interestingly, some residual domains persist well beyond

the apparent saturation field determined from the hysteresis loop. These domains, if not annihilated, impede the avalanche-like domain propagation during the subsequent field cycle and manifest themselves as distinct features in the FORC diagram. The number of unannihilated domains depends on the maximum reversal field applied. Thus it is not trivial to determine the true saturation field of the system from the major hysteresis loop alone. Our results illustrate detailed magnetization reversal processes in Co/Pt and provide direct and quantitative measures of the true saturation field and other reversal characteristics.

II. Experimental Procedures

The perpendicular films used for our experiments are $[Co(4Å)/Pt(7Å)]_{50}$ multilayers that were simultaneously magnetron-sputtered onto Si_3N_x-coated Si substrates (for magnetometry measurements) and Si_3N_x-membranes (for the TXRM and SAS measurements in transmission mode). A 200-Å Pt buffer layer and a 20-Å Pt capping layer have been used. The perpendicular easy axis in the system is obtained via the high surface anisotropy of the 4-Å Co layers. The Pt buffer layer and the multilayer are (111) textured. More detailed information about the samples can be found in prior publications [12-14].

Magnetization reversal on the macroscopic scale has been measured by Magneto-Optical Kerr Effect (MOKE) and by the FORC method utilizing a Princeton Measurements Corporation 2900 Alternating Gradient Magnetometer (AGM) at room temperature with the magnetic field applied perpendicular to the sample. The AGM is used to measure a large number ($\sim 10^2$) of partial hysteresis curves called First-Order Reversal Curves (FORCs) in the following manner. After saturation, the magnetization M

is measured starting from a reversal field H_R back to positive saturation, tracing out a FORC. A family of FORCs is measured at different H_R, with equal field spacing, thus filling the interior of the major hysteresis loop (Fig. 1a). Since the FORC technique uses a large data set in comparison to the usual single major hysteresis loop, it can reveal much more detailed information about the reversal. If the magnetization at the applied field H on the FORC with reversal field H_R is defined as $M(H_R, H)$, a FORC distribution is then defined by a mixed second order derivative: $\rho(H_R, H) \equiv -\frac{1}{2}\frac{\partial^2 M(H_R, H)}{\partial H_R \partial H}$ [7-9]. This derivative eliminates the purely reversible components of the magnetization. A plot of the distribution ρ versus H and H_R can then be created to probe the details of the magnetization reversal.

In order to correlate the macroscopic information obtained by FORC with the microscopic evolution of specific domain patterns, we perform TXRM and SAS on similar samples grown onto Si_3N_x-membrane substrates. The magnetic contrast is obtained from the resonant magnetic term in the atomic scattering factor that is first order in the magnetization [X-ray Magnetic Circular Dichroism (XMCD)] [15, 16]. Such techniques are excellent tools for microscopic reversal studies since this photon-in-photon-out method does not perturb the sample during measurement as compared to Magnetic Force Microscopy (MFM) and is insensitive to external fields applied to the sample. This is especially important for studying domain nucleation and annihilation processes in an external magnetic field. X-ray measurements were performed at the Advanced Light Source (ALS) at the Lawrence Berkeley National Laboratory. The TXRM imaging used the XM-1 zone-plate imaging microscope on bending magnet beamline 6.1.2 while the SAS was performed on beamline 8.0. To enhance the magnetic contrast we tuned the energy to the Co L_3 absorption edge (~ 778 eV, ~ 1.59 nm). The

imaging was done with a 2-dimensional CCD camera using elliptical polarization from above the synchrotron orbit plane in applied fields up to 3.5 kOe [15, 16]. The SAS was performed using linear polarization [17]. Both techniques are applied in transmission and are predominantly sensitive to the perpendicular magnetization of the sample.

III. Experimental results

A. FORC

The experimentally-obtained family of the FORCs for a $[Co(4Å)/Pt(7Å)]_{50}$ sample is shown in Fig. 1a where the outer boundary delineates the major hysteresis loop. Five reference points are marked to illustrate the different reversal stages. The major loop is characteristic of magnetic thin films with perpendicular magnetic anisotropy as first outlined by Kooy and Enz [18]. The initial stage of the reversal is the nucleation and propagation of reverse domains (point 1 of Fig. 1a). Once these domains fill the sample the magnetization is characterized by mostly reversible changes of the "up" vs. "down" domain widths (between points 2 and 3), while the overall domain topology is preserved. Finally, saturation occurs via annihilation of residual unswitched domains (points 4 to 5). The corresponding FORC distribution plotted versus H and H_R is shown in Fig. 1b and 1d as a contour plot and a 3-dimensional plot, respectively. For each curve shown in Fig. 1a with a specific reversal field H_R, the magnetization M is measured with increasing applied field H; the corresponding FORC distribution ρ is represented by a horizontal line scan at that H_R along H. Five line-scans corresponding to the reference points in Fig. 1a are represented by dashed lines in Fig. 1b. As H_R decreases and the family of FORCs are measured, ρ is scanned in a "top-down" fashion in the H-H_R plane, mapping out the irreversible processes. We observe three regions of interest in the FORC distribution in

Fig. 1b and 1d: a horizontal ridge in the upper right corner, an intermediate mostly flat region with little FORC features, and finally a vertical valley/peak pair in the lower left corner.

The first feature is a ridge along the applied field direction. A vertical cross-sectional view of this feature (Fig. 1c) shows that the ridge rises abruptly as H_R is decreased from the $\rho = 0$ plane above the ridge. When magnetization reversal processes are completely reversible, the magnetization $M(H_R, H)$ would not change from reversal curve to reversal curve, or successive reversal curves will overlap. Therefore it can be solely expressed as a function of the applied field H, and not the reversal field H_R. Thus the FORC distribution goes to zero in these regions. That is,

$$\rho = -\frac{1}{2}\frac{\partial^2 M(H_R, H)}{\partial H_R \partial H} = -\frac{1}{2}\frac{\partial^2 M(H)}{\partial H_R \partial H} = 0 \qquad (1)$$

for reversible processes.

The rise of the ridge corresponds to the FORC distribution becoming nonzero, signaling the onset of irreversible processes. This onset is better seen in the projection of the FORC distribution onto the H_R axis (equivalent to integrating ρ over H): for the entire ridge, we take a series of equally spaced cross sectional cuts along H, spanning the ridge and summing them together. Then a line fit is done along the right side of the ridge, as shown in Fig. 1c, where the intersection between the line fit and the horizontal axis indicates the onset of irreversibility. The onset determined this way is 1.4 kOe. It can readily be seen in Fig. 1a that this field (point 1) indeed corresponds to where the magnetization drops precipitously, signaling an avalanche-like growth of reverse domains in the film. After the ridge has peaked, ρ returns gradually to the $\rho = 0$ plane. The endpoint of the irreversible switching (point 2) can be similarly determined to be about

1.2 kOe. This first irreversible ridge in Fig. 1b also reflects the sudden separation in the successive reversal curves visible in Fig. 1a.

The second feature in Fig. 1b is a planar region between lines 2 & 3 (-2.5kOe $< H_R <$ 1.2kOe), separating the aforementioned horizontal ridge from a vertical pair of a valley/peak-feature. In this region, ρ is essentially zero and invariant in the H_R-H plane, indicating mostly reversible switching (Fig. 1d) [19]. The successive FORCs in Fig. 1a are indeed closely packed and nearly overlap. The reversibility of the sample in this region has been also observed using TXRM, which shows that the domains fill the sample and reversibly widen and narrow as the field is varied around remanence [13].

The third feature consists of a negative valley and a positive peak in ρ that stretch in the nearly vertical direction, between lines 3 & 5 (-3.8 kOe $< H_R <$ -2.5 kOe). The onset of this feature indicates the reintroduction of significant irreversible processes showing domain annihilation as the sample approaches negative saturation. At -3.2 kOe (point 4 in Fig. 1a), the major loop appears to have reached negative saturation, and one might expect this would simultaneously declare the end of the irreversible switching. Strikingly, the FORC distribution is far from vanishing (line 4 in Fig. 1b). In fact this is just the beginning of a negative/positive pair of peaks.

A careful examination of the reversal curves in Fig. 1a shows that reversing from the apparent saturation (point 4) leads to a rounded corner in the returning path, in contrast to the sharp nucleation edge seen in the major loop. Furthermore, for -3.8 kOe $< H_R <$ -3.2 kOe (between points 4 & 5), the negative FORC distribution in $H <$ -1.4 kOe (Fig.1b & 1d) corresponds to a decrease of the FORC slope (Fig.1a); the positive FORC distribution in $H >$ -1.4 kOe (Fig.1b & 1d) corresponds to an increase of the FORC slope (Fig.1a). Hence this negative/positive pair of peaks represents the formation of a sharp

corner that is present in the return path of the major loop. These results show that irreversible switching persists well beyond the perceived major-loop saturation field of -3.2 kOe for this sample, and the larger (or more negative) the reversal field H_R, the more abrupt the subsequent reversal. In this region the macroscopic magnetization differs by less than 1 μemu, the resolution of our measurement, or 0.7% of the saturation moment. However, the small residual moments are reflected in dramatic differences in the nucleation stage during the subsequent reversal.

B. Transmission X-ray Microscopy

To explore these macroscopic reversal stages, we use the TXRM technique to image and follow the domain patterns on the microscopic scale. In Fig. 2 we exhibit the hysteresis loop of the sample used for TXRM imaging which has nominally the same structure as the one shown in Fig.1a. The loops are nearly identical, however the TXRM sample has slightly lower nucleation and saturation fields resulting from sample-to-sample variations in deposition. For this sample we show in Fig. 2 a series of representative TXRM images, over a 2.2 x 2.2 μm^2 area, taken along a field sweep from positive to negative saturation. The dark/bright contrast illustrates the opposite "up"/ "down" domains. The decreasing-field branch of the hysteresis loop is color-coded (on-line) corresponding to the different reversal stages identified below.

Initially, the sample is fully saturated beyond $H \sim 3.5$ kOe, on both macroscopic and microscopic level (segment *a*, black online). As a reversal field is applied, even in the apparent macroscopic saturation state and well above the apparent nucleation field (1.3kOe < H <3.0kOe), we begin to observe isolated nucleation of a few reverse domains. We first observe 0-dimensional spot-like bubble domains (typically 1-3 nucleation

sites/100 μm^2 area) that grow in size with decreasing field (segment *b*, green online) but remain as bubbles. As the field is further reduced the 0-dimensional domains expand into 1-dimensional isolated stripes (~ 1.1 kOe, segment *c*).

At the sharp edge in the major loop, where the FORC diagram begins to display irreversible switching, we observe a sudden avalanche of labyrinth stripe domains, seeded from the few isolated reverse domains already present. These avalanches move through the whole sample very quickly (segment *d*, yellow online) and a characteristic domain periodicity develops. This process corresponds to the horizontal FORC ridge over a narrow H_R range (between lines 1 & 2 in Fig. 1b). Thus, the sharp drop in magnetization and the onset of irreversible behavior are not directly associated with the nucleation of new reverse domains, but primarily with the sudden growth of already present stripe domains.

Next the magnetization decreases almost linearly with decreasing field (segment *e*, red online). The sample is now filled with labyrinth stripe domains. The decrease in *M* is due to a relative change in the width of "up" vs. "down" domains. In this stage the topology of the domains is preserved (see the three images at 0.5, -0.2 and -1.8 kOe in Fig. 2) and the ratio of white versus dark regions agree very well with the macroscopic magnetization. This corresponds to the second feature in the FORC diagram, the planar region, where we observe mostly reversible switching.

Continued reversal leads to a steeper drop in *M* approaching negative saturation (segment *f*, yellow online). Microscopically, the domains start to contract and annihilate. Compared to the earlier nucleation stage, there are now much more isolated domains per area present towards saturation. Near the apparent saturation (segment *g*, blue online, e.g., at -2.8 kOe), there are still isolated 1-dimensional stripe domains and 0-dimensional

bubble domains present, even though the magnetic moment associated with them becomes negligible. Beyond the apparent saturation (segment *h*, green online, e.g., at -3.3 kOe), the 0-dimensional bubble domains persist, and they continue to contract in size down below the TXRM resolution limit (however they are still present in the samples as we will show below). These segments together correspond to the third region in the FORC diagram, the irreversible valley/peak feature. Eventually a true negative saturation is achieved (segment *i*, black online).

We look more closely at the saturation of the magnetization in Fig. 3. In the background we show the third quadrant of a major hysteresis loop when reversing at -4.0 kOe (solid line), together with a hysteresis loop reversing at -3.1 kOe (open circles), which appears sufficient to saturate the sample. However, in the subsequent reversal this second loop has a gradual corner near -1.2 kOe, deviating appreciably from the sharp edge seen in the major loop (similar to the FORCs in Fig. 1a). In order to reveal the microscopic domain structures associated with this feature, we exhibit two sets of TXRM images taken along that second loop in Fig. 3: one at -2.5 kOe along the decreasing-field branch before negative saturation (a & b), and the other at -1.8 kOe along the increasing-field branch after reversing at -3.1 kOe (c & d). As shown in Fig. 3a, approaching negative saturation, there is a mixture of isolated stripe and bubble domains. When reversing from -3.1 kOe, at -1.8 kOe, we observe a number of bubble domains (Fig. 3c), which can be traced to the domains in Fig. 3a. To highlight this we have marked the positions of the bubble domains in Fig. 3c with open circles (Fig. 3d). These same circles are then superimposed onto Fig. 3a, and the resultant composite graph is shown in Fig. 3b. The circles in Fig. 3b highlight either bubble domains or ends of residual stripe domains. Clearly all the bubble domains in Fig. 3d after reversal have originated from

residual domains in Fig. 3b approaching saturation. Interestingly, at -3.1 kOe, some of the bubble domains apparently have vanished as they contract below the resolution limit of the microscope. Yet they have not been truly annihilated and reappear during the subsequent increasing field sweep.

The number of such bubble domains nucleated during the early stage of the subsequent reversal, where the major hysteresis loop still appears as saturated, provides measure for the number of unannihilated residual domains (even if their sizes are below the imaging resolution) at the maximum applied reversal field. We can repeat the process shown in Fig. 3 for other maximum reversal fields, and simply count the number of nucleated bubble domains at -1.5 kOe within a certain image area. As shown in Fig. 4, at increasingly negative reversal fields, the number of bubble domains gradually decreases, suggesting a rather slow approach towards true saturation.

Each of these bubble domains then nucleates separately stripe domains that later propagate to the entire sample, corresponding to the edge in the major hysteresis loop. It is clear that the smaller the maximum reversal field is, the larger the number of unannihilated residual domains, and the more gradual becomes the avalanche-like domain propagation process. In essence, there is less and less space left for each individual avalanche if the number of nucleation sites increases. Eventually the avalanching is suppressed completely and we observe a gradual rather than a sudden domain growth. This is better shown in Fig. 5, where two sets of images are compared at the same field after the sample has been exposed to different maximum reversal fields of 3.5 and 2.9 kOe, respectively. Note that the domain patterns near positive saturation are representative of those near negative saturation discussed in Figs. 3 & 4, as these samples exhibit complementary point memory effect [20]. When exposed to a field of 3.5 kOe,

only very few nucleation sites are seen prior to the sharp magnetization drop (left panels of Figs. 5a & 5b). When exposed to a field of 2.9 kOe, many more nucleation sites are seen leading to the gradual magnetization drop (right panels of Figs. 5a & 5b, and Fig. 5d). After the stripe domains have propagated, the domain patterns are similar (Fig. 5c).

C. Resonant small angle scattering

To further confirm the slow saturation of residual domains we complement the TXRM imaging results with resonant SAS. Scattering is not limited by the imaging resolution and is sensitive to magnetic heterogeneities of size comparable to the x-ray wavelength (~1.6 nm). The field dependence of the magnetic scattering intensity from the Co/Pt multilayer is shown in Fig. 6a and is similar to that shown in Ref. 17. The SAS loop is measured with the detector set such that there is an in-plane scattering wave vector q = 0.024 nm^{-1}. The scattered intensity results from deviations from the average magnetization and is proportional to the square of the Fourier transform of the magnetization distributions. The features in the SAS loop correlate closely with features in the hysteresis loop shown in Fig. 2. Beyond saturation, the magnetization of the sample is uniform and the scattering is at a minimum. As the field is reduced scattering commences at the nucleation point and increases its intensity by orders of magnitude to a maximum near the coercive field before falling back to the saturation level again at the opposite saturation. As shown in Fig. 6a, the apparent nucleation and saturation fields are around ±2.8 kOe and ±1.2 kOe, respectively, coinciding with the onset and completion of reversal as inferred from the major hysteresis loop (Fig. 2).

However, at an expanded scale shown Fig. 6b, the slow approach to saturation becomes apparent. A small but measurable scattering intensity originating from the

residual bubble domains is reflected in this reversal profile. As the system approaches saturation, the reduction in scattering intensity can occur both from the reduction of the bubble domain size and from the annihilation of the bubble domains, which cannot be easily distinguished. However, it is clear from the SAS measurements that significantly higher fields are required to fully saturate the sample, in agreement with the FORC and TXRM results. For the example in Fig. 6b, fields exceeding -4.0 kOe are required to reach the saturated scattering intensity whereas the saturation appears much earlier on the full intensity scale (Fig. 6a) and the hysteresis loop, near -2.8 kOe. Similarly, on reduction of the field, the first increase in scattering signaling the formation of reverse domains occurs near -2.0 kOe, well before the pronounced increase in scattering that signals the avalanche of reverse domains at -1.2 kOe. This, again, corresponds nicely with the imaging results in Fig. 2 where bubble domains are observed well before the formation of the stripe domain pattern.

IV. Discussion and conclusion

The observed microscopic magnetization reversal processes resemble those seen in other systems with perpendicular anisotropy, such as garnet, CoCr, and Co/Pd films [13, 18, 21-23]. Towards saturation, the labyrinth domains contract to form isolated stripe domains that contract further into bubble domains. Eventually the bubble domains collapse at a critical field H_{bc} and a true saturation is reached. Theoretically, H_{bc} can be calculated, according to

$$H_{bc} = 4\pi M_S - 8\sqrt{\sigma_W / D(1+\sqrt{\mu})}\,, \qquad (2)$$

where M_S, σ_W, D, and μ are saturation magnetization, domain wall energy density, film thickness, and permeability, respectively [18]. For the present Co/Pt multilayers we

estimate H_{bc} ~ -3.4 kOe [24]. Experimentally, the bubble collapse field H_{bc} has been difficult to measure. Macroscopically, the major hysteresis loop is not sensitive enough to reflect the small fractions of un-reversed bubble domains; microscopically, the bubble domains can contract below the resolution limit of the magnetic imaging techniques, making the precise determination of H_{bc} difficult. In contrast, the FORC distribution, the second order derivative of magnetization, is very sensitive to this collapse field. Before saturation, any residual bubble domains result in increased irreversibility in the subsequent field sweep, giving rise to a non-zero ρ. Only after reaching a true saturation the subsequent field sweep will become H_R-independent, or ρ=0. As shown earlier, the true saturation field determined by FORC is H_S ~ -3.8 kOe. Note that it is not unexpected that H_S is slightly different from H_{bc}: Equation (2) calculates an *average* H_{bc} based on the known material characteristics of a homogeneous sample; The FORC H_S reflects the *actual* H_{bc} which is modified by inhomogeneities. The determination of this true saturation field is important for the application of such materials in perpendicular magnetic recording, where old data needs to be overwritten by the recording head.

Reviewing the microscopic analysis of the reversal via TXRM and SAS and the macroscopic analysis with FORC, it seems that nucleation and saturation are almost two inversely symmetric processes: both are macroscopically irreversible; one creates, while the other annihilates domains. In addition, both exhibiting microscopic domains well before the macroscopic nucleation and well beyond macroscopic saturation points that would be typically identified from the major hysteresis loop. On the other hand there are clear asymmetries. Irreversible FORC features are visible beyond macroscopic saturation, but are not sensitive to the reversal domain formation before macroscopic nucleation. This originates from the fact that there is no minor loop visible before macroscopic

nucleation, since the moment connected with the few domains present at that stage is below the instrumental resolution. In contrast, the lack of saturation due to residual domains becomes significantly amplified due to its impact on the domain avalanches during the subsequent nucleation (sharp edge in the hysteresis loop becomes gradual), as shown in Figs. 3 and 5. We also observe that the density of isolated nucleation sites after "microscopic saturation" is much lower than the density of isolated residual domains just before saturation, i.e. the tendency to fracture into isolated domains is rather high towards saturation: we typically observe about 200 isolated domains /10μm^2, while only very few isolated domains trigger nucleation (typically only 1-3 domains /10μm^2).

In conclusion, we have analyzed the magnetic reversal of Co/Pt multilayers using a complementary combination of macroscopic FORC and microscopic TXRM and SAS techniques. A striking feature of the system is that irreversible switching processes can persist well beyond the apparent saturation, where the macroscopic magnetization levels off. We find that in that stage a small but crucial amount of residual reverse domains are still present. While not readily observed in the major loop, these residual domains alter the subsequent minor loop reversal process significantly since they provide the nucleation sites for the avalanche-like growth of the stripe domains. As a result the residual domains produce a characteristic feature in the FORC distribution that has no counterpart in the major loop. Our results also demonstrate that the FORC method is a sensitive macroscopic technique (particularly in the $H–H_R$ coordinate system) for probing the reversibility/irreversibility of magnetic switching processes in perpendicular magnetic multilayers. Combined with TXRM and SAS, it is possible to obtain a comprehensive and quantitative understanding of magnetic reversal processes.

Acknowledgement

Work at UCD has been supported by Lawrence Livermore National Laboratory UCDRD funds. The acquisition of an alternating gradient magnetometer which was used extensively in this investigation was supported by NSF Grant No. EAR-0216346. G.D., J.B.K., and work at LBNL have been supported by the Director, Office of Science, Office of Basic Energy Sciences of the U.S. DOE under Contract DE-AC03-76SF00098. We thank C. P. Pike, G. Acton, A. Roth, K. L. Verosub, R. T. Scalettar, G. T. Zimányi, M. S. Pierce, C. R. Buechler, and L. B. Sorensen for helpful discussions.

References

* kailiu@ucdavis.edu.

1. For a recent review, see e.g., J. I. Martín, J. Nogués, K. Liu, J. L. Vicent, and I. K. Schuller, J. Magn. Magn. Mater. **256**, 449 (2003).
2. E. E. Fullerton, J. S. Jiang, and S. D. Bader, J. Magn. Magn. Mater. **200**, 392 (1999).
3. M. D. Stiles and R. D. McMichael, Phys. Rev. B **59**, 3722 (1999).
4. V. I. Nikitenko, V. S. Gornakov, A. J. Shapiro, R. D. Shull, K. Liu, S. M. Zhou and C. L. Chien, Phys. .Rev. Lett. **84**, 765 (2000).
5. L. Savtchenko, B. N. Engel, N. D. Rizzo, M. F. Deherrera, J. A. Janesky, US Patent 6,545,906 B1.
6. G. M. McClelland, M. W. Hart, C. T. Rettner, M. E. Best, K. R. Carter, and B. D. Terris, Appl. Phys. Lett. **81**, 1483 (2002).
7. C. R. Pike, A. Roberts, and K. L. Verosub, J. Appl. Phys. **85**, 6660 (1999).
8. H. G. Katzgraber, F. Pázmándi, C. R. Pike, Kai Liu, R. T. Scalettar, K. L. Verosub, and G. T. Zimányi, Phys. Rev. Lett., **89**, 257202 (2002).
9. C. R. Pike, Phys. Rev. B, **68**, 104424 (2003).
10. A. Stancu, C. Pike, L. Stoleriu, P. Postolache, and D. Cimpoesu, J. Appl. Phys. **93**, 6620 (2003).
11. D. Weller, L. Folks, M. Best, E. E. Fullerton, B. D. Terris, G. J. Kusinski, K. M. Krishnan, and G. Thomas, J. Appl. Phys. **89**, 7525 (2001).
12. O. Hellwig, S. Maat, J. B. Kortright, and E. E. Fullerton, Phys. Rev. B **65**, 144418 (2002).
13. O. Hellwig, G. P. Denbeaux, J. B. Kortright, and E. E. Fullerton, Physica B **336**, 136 (2003).

14. M. S. Pierce, R. G. Moore, L. B. Sorensen, S. D. Kevan, O. Hellwig, E. E. Fullerton, and J. B. Kortright, Phys. Rev. Lett. **90**, 175502 (2003).

15. J. B. Kortright, D. D. Awschalom, J. Stöhr, S. D. Bader, Y. U. Idzerda, S. S. P. Parkin, I. K. Schuller, and H.-C. Siegmann, J. Magn. and Magn. Mater. **207**, 7 (1999).

16. P. Fischer, G. Denbeaux, T. Eimüller, D. Goll, and G. Schütz, IEEE Trans. Mag. **38**, 2427 (2002).

17. J. B. Kortright, S. K. Kim, G. P. Denbeaux, G. Zeltzer, K. Takano, and E. E. Fullerton, Phys. Rev. B **64**, 092401, (2001).

18. C. Kooy and U. Enz, Philips Res. Repts. **15**, 7 (1960).

19. The 45º line in Fig. 1b between reference lines 1 & 3 represents the boundary of our data set.

20. M. S. Pierce, C. R. Buechler, L. B. Sorensen, J. J. Turner, S. D. Kevan, E.A. Jagla, J.M. Deutsch,T. Mai, O. Narayan, J. E. Davies, K. Liu, J. Hunter Dunn, K. M. Chesnel, J. B. Kortright, O. Hellwig, and E. E. Fullerton, Phys. Rev. Lett., in press (cond-matt/0411698).

21. F. Schmidt and A. Hubert, J. Magn. Magn. Mater. **61**, 307 (1986).

22. A. Hubert and R. Schäfer, *Magnetic Domains* (Springer-Verlag, Berlin, 1998).

23. A. W. Rushforth, P. C. Main, B. L. Gallagher, C. H. Marrows, B. J. Hickey, E. D. Dahlberg, and P. Eames, J. Appl. Phys. **89**, 7534 (2001).

24. Based on M_S= 700 emu/cm^3, anisotropy K= 3 x 10^6 erg/ cm^3, σ_W =6 erg/cm^2.

Figure Captions:

Fig. 1. (Color online) a) A family of first order reversal curves for a $[Co(4Å)/Pt(7Å)]_{50}$ sample, where the first point of each reversal curve is shown by a black dot, and b) a contour plot and d) a 3-dimensional plot of the corresponding FORC distribution, versus applied field H and reversal field H_R. Reference points 1-5 are marked in a) and b) to illustrate the different reversal stages. c) shows the projection of the horizontal FORC ridge in b) onto the H_R axis (sum of vertical cross-sectional cuts taken along the horizontal ridge), with dashed lines drawn to determine onset and endpoint of irreversibility.

Fig. 2: (Color online) Kerr hysteresis loop with TXRM images along a field reversal of a $[Co(4Å)/Pt(7Å)]_{50}$ multilayer. The different stages of the reversal process from positive to negative saturation are represented by several segments of the major loop, *a*-*i*, as described in the text. The different TXRM images, over the same 2.2 x 2.2 μm^2 area of the sample, exhibit the characteristic domain pattern evolution during reversal. Approximate external fields, within ±0.1kOe, are given for each image and are also marked on the hysteresis loop. TXRM images and corresponding marks on the hysteresis loop are connected by arrows.

Fig. 3: Partial Kerr hysteresis loop around negative saturation. The solid line is part of the major hysteresis loop, with a maximum reversal field of -4.0 kOe. Open symbols represent part of a loop reversed at -3.1 kOe. TXRM images are shown in (a-d), over a same 2.7 μm x 5.2 μm area of the sample, at -2.5 kOe approaching saturation (a,b) and at

-1.8 kOe (c,d) after exposure to a -3.1 kOe field. The open circles in image d) mark the nucleation sites of image c), and coincide with the residual white reverse domains before saturation in image a). The composite is shown in image b).

Fig. 4: Number of nucleation sites (y-axis) observed within a 12 μm diameter circle, after bringing the sample from positive saturation to a maximum negative reversal field, whose value is plotted on the x-axis, and then reducing the field back to -1.5 kOe for imaging.

Fig. 5: (a-c) Comparison of three pairs of TXRM images (all 5.6 μm x 4.5 μm), each pair of images collected at the same external field (a = 1.5 kOe, b = 1.2 kOe and c = 0.9 kOe) after exposing to different maximum reversal fields of 3.5 and 2.9 kOe for the left and right panel of each pair, respectively. d) shows the first quadrant of the corresponding MOKE hysteresis loops reversed at 2.9 kOe (open symbols) and 3.5 kOe (solid symbols). The fields at which the TXRM images (a-c) are taken are also marked by larger open and solid circles.

Fig. 6: (a) Resonant magnetic soft X-ray scattering intensity profiles from a $[Co(4Å)/Pt(7Å)]_{50}$ multilayer over a complete field cycle. (b) A plot zooms in on the saturation and nucleation details as marked by the grey box in (a). The solid and open symbols represent the decreasing-field and increasing-field branch, respectively, as indicated by the arrows. The magnified view in (b) reveals a gradual intensity drop towards saturation and a gradual increase at nucleation reflecting the residual domains present at these fields.

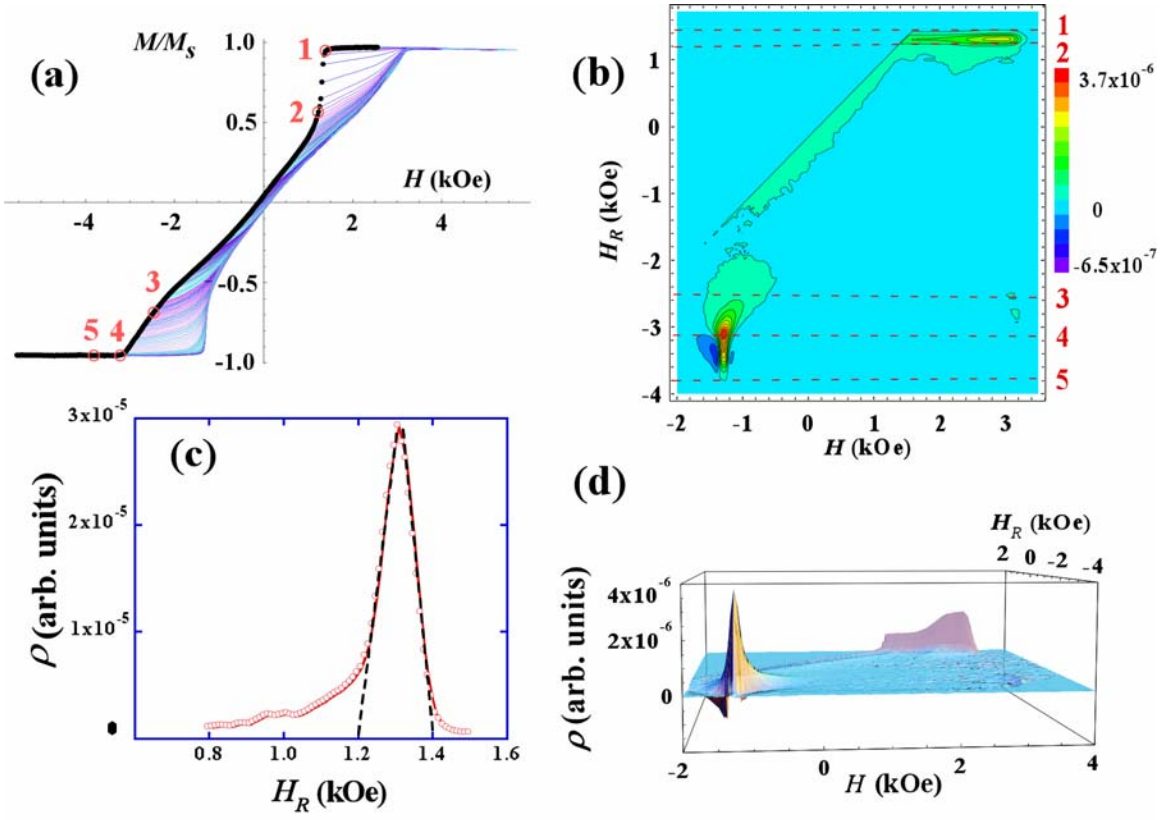

Fig. 1 (To publish in double columns)

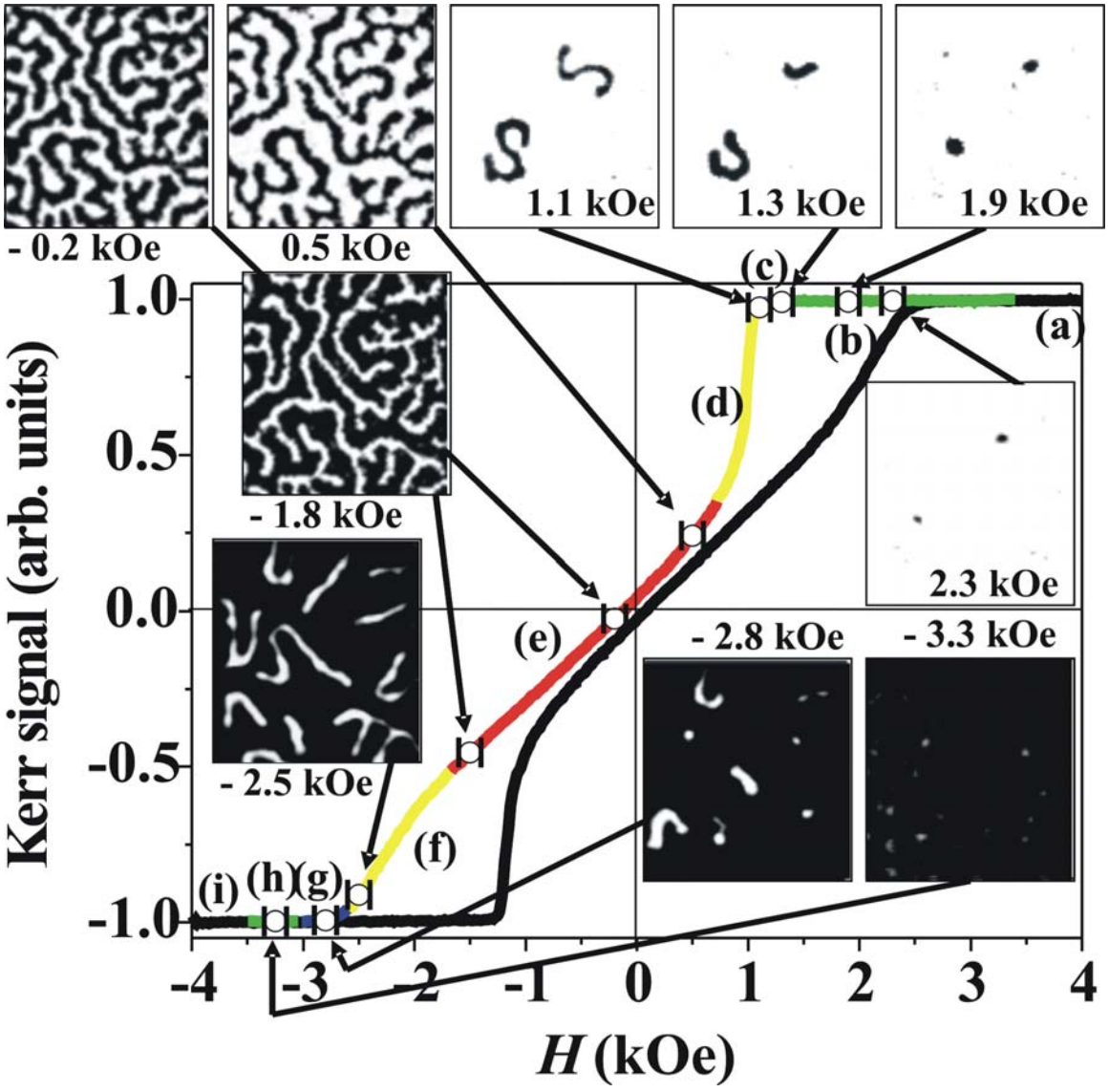
- 0.2 kOe
0.5 kOe
1.1 kOe
1.3 kOe
1.9 kOe
(c)
(b)
(a)
(d)
- 1.8 kOe
2.3 kOe
(e)
- 2.8 kOe
- 3.3 kOe
- 2.5 kOe
(f)
(i)
(h)
(g)
1.0
0.5
0.0
-0.5
-1.0
Kerr signal (arb. units)
-4
-3
-2
-1
0
1
2
3
4
H (kOe)

Fig. 2

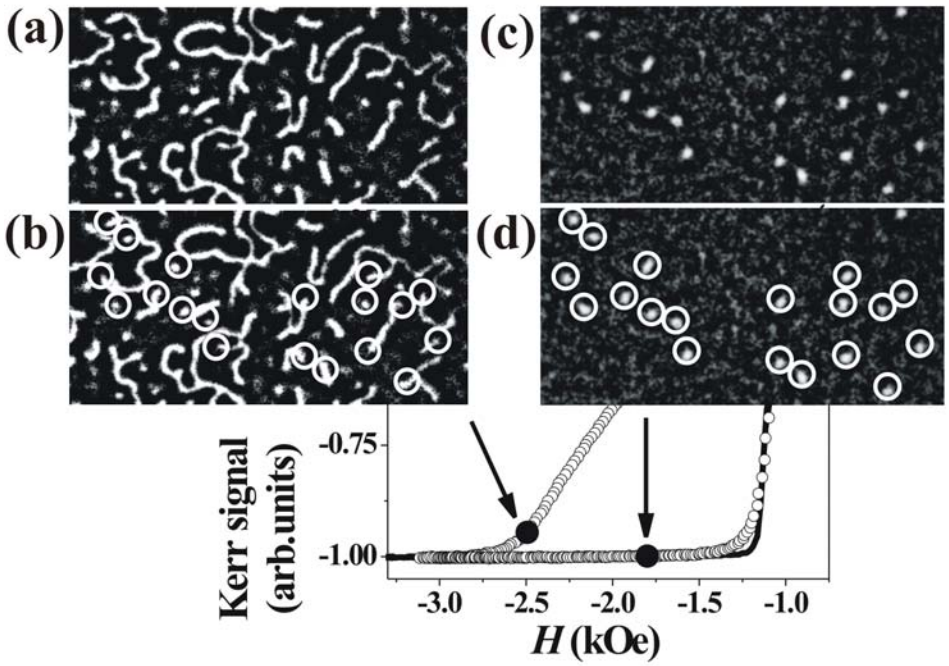

Fig. 3

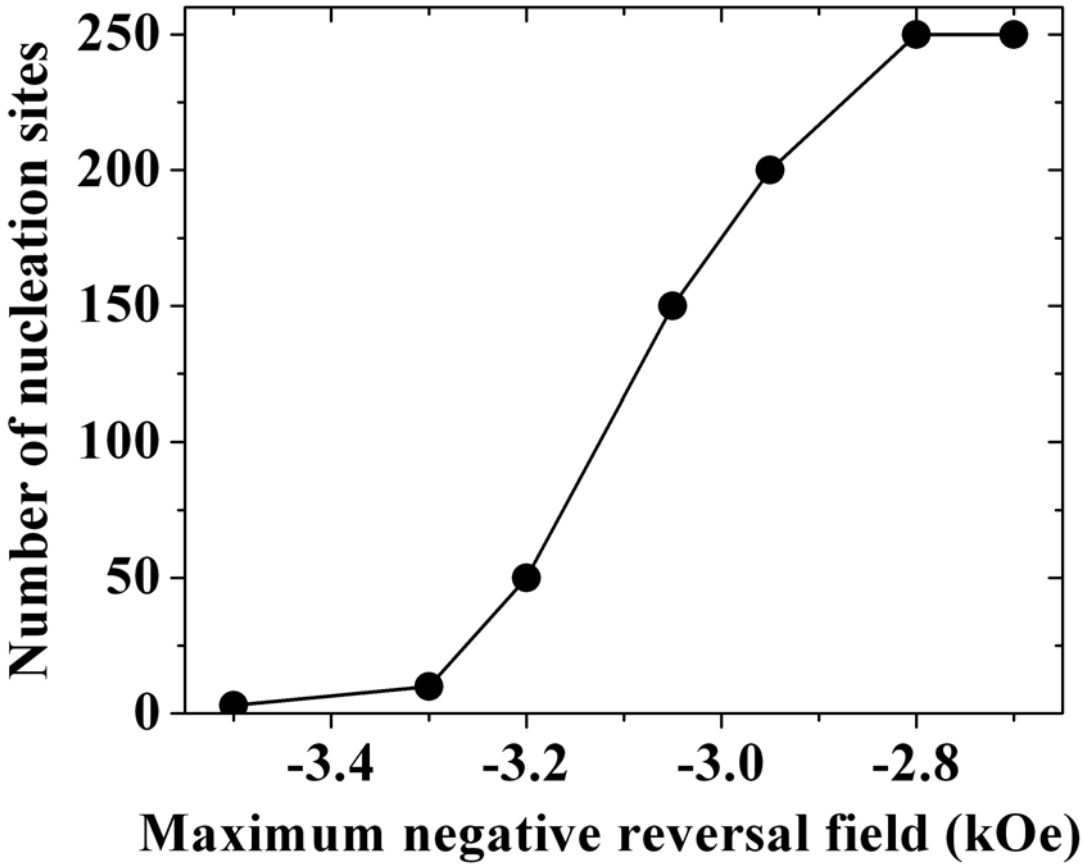
Number of nucleation sites
250
200
150
100
50
0
-3.4
-3.2
-3.0
-2.8
Maximum negative reversal field (kOe)

Fig. 4

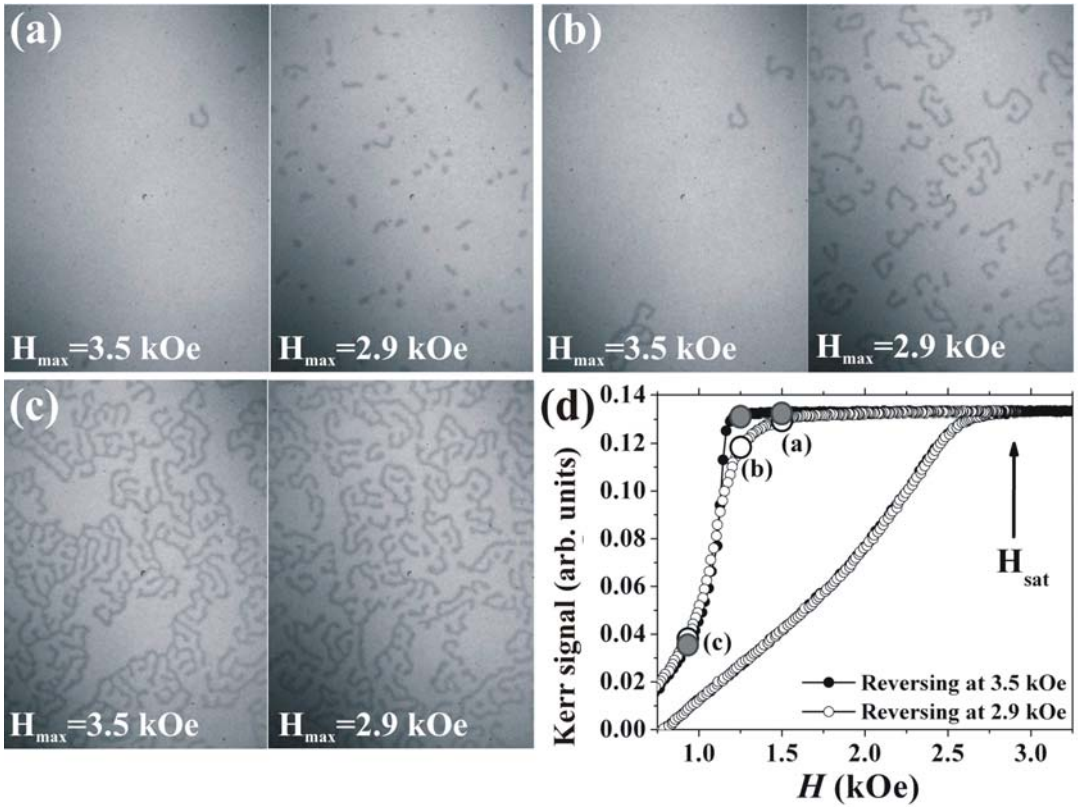
(a)
H_max=3.5 kOe
H_max=2.9 kOe
(b)
H_max=3.5 kOe
H_max=2.9 kOe
(c)
H_max=3.5 kOe
H_max=2.9 kOe
(d)
Kerr signal (arb. units)
0.14
0.12
0.10
0.08
0.06
0.04
0.02
0.00
(a)
(b)
(c)
H_sat
Reversing at 3.5 kOe
Reversing at 2.9 kOe
1.0
1.5
2.0
2.5
3.0
H (kOe)

Fig. 5

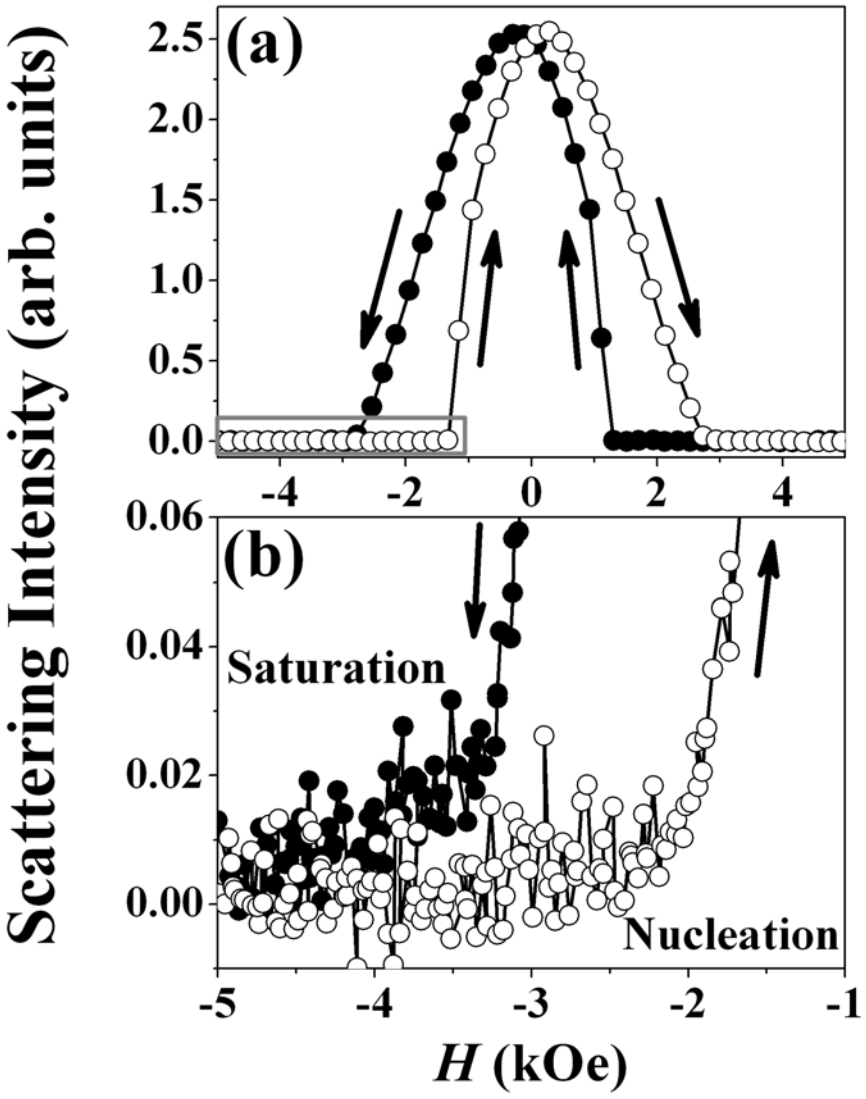
Scattering Intensity (arb. units)
(a)
2.5
2.0
1.5
1.0
0.5
0.0
-4
-2
0
2
4
(b)
0.06
0.04
0.02
0.00
Saturation
Nucleation
-5
-4
-3
-2
-1
H (kOe)

Fig. 6